Developmental plasticity to high light intensity amplifies the advantage of amphistomous leaves

Christopher D. Muir[1,2*] Wei Shen Lim[1] Dachuan Wang[1,2]

[1]School of Life Sciences, University of Hawai'i, Mānoa, Hawai'i, USA
[2]Department of Botany, University of Wisconsin, Madison, Wisconsin, USA

*Corresponding author: cdmuir@wisc.edu

ORCID: Christopher D. Muir — 0000-0003-2555-3878

Abstract

The presence of stomata on both leaf surfaces (amphistomy) can increase photosynthesis in C_3 plants by reducing the path length for CO_2 diffusion between substomatal cavities and chloroplasts. Amphistomatous leaves are common among herbaceous plants growing in sunny habitats, including many crop species. This distribution of amphistomatous leaves in nature may result from an increased photosynthetic benefit of amphistomy under high light intensity, either because of acclimatory, plastic, or constitutive variation in CO_2 supply or demand. We used a recently developed method to quantify amphistomy advantage, the photosynthetic rate of an amphistomatous leaf relative to an otherwise identical hypostomatous leaf, in 29 diverse populations representing 14 species of wild tomatoes (*Solanum* sect. *Lycopersicon* and sect. *Lycopersicoides*). Plant grown under high light intensity benefit more in terms of CO_2 assimilated for a given stomatal conductance than plants grown under low light, regardless of measurement light intensity or native light habitat. Developmental plasticity in leaf thickness and/or density, an adaptive response to optimize light interception, likely affects CO_2 diffusion within the leaf, altering amphistomy advantage as a byproduct. Developmental plasticity may therefore play an important and previously unnoticed role in explaining the adaptive significance of amphistomy and the distribution of amphistomatous leaves in nature.

Main text

Stomata are microscopic pores on the surfaces of leaves and other photosynthetic organs formed by a pair of guard cells. They are essential for balancing carbon gained per unit water lost and permitted vascular plants to grow tall on land by enabling access to CO_2 for photosynthetic carbon assimilation

while preventing hydraulic failure in variable environments (*1–3*). Optimal stomatal function depends on both dynamic changes in aperture on the scale of minutes to hours, as well as static anatomy determined by developmental plasticity and constitutive genetic differences (*4–6*). Understanding how stomata respond to environmental change over daily, developmental, and evolutionary time is important for understanding adaptation (*1*, *7–12*), predicting paleoclimate from fossil cuticles (*13–15*), and improving crops (*16*). Stomatal function contributes to global carbon and water cycles (*17*) and therefore predicting future climate (*18*).

Despite extensive theoretical and empirical progress understanding stomata function and anatomy from molecular to ecosystem levels, the adaptive significance of amphistomatous leaves remains an important unsolved problem in leaf structure-function relationships (*19–26*). Amphistomatous leaves develop abaxial and adaxial stomata whose aperture can be independently regulated (*27–31*) to control gas exchange through each surface. All else being equal, gas exchange through stomata on both surfaces increases CO_2 supply to chloroplasts by providing a second parallel pathway through leaf intercellular airspaces, enhancing photosynthesis (*20*, *32*). The extent to which amphistomy increases CO_2 supply depends on resistance to diffusion in intercellular airspaces. This resistance can be low in thin, porous, amphistomatous leaves (*28*, *33*), but may be more substantial in thick, dense, hypostomatous leaves (*34*). Amphistomatous leaves also lose more water through evaporation because of a second boundary layer conductance (*35*), but the additional carbon gain should be enough to offset this cost in most realistic scenarios (*36*).

The paradoxical fact is that, despite the photosynthetic benefit, most leaves are not amphistomatous. Many vertically oriented and/or isobilateral leaves are amphistomatous (*25*). But among dorsiventral leaves, herbaceous plants in open, high light habitats tend to have have amphistomatous leaves (*22*, *39–44*). Most other leaves, except those from aquatic habitats, are hypostomatous, producing stomata only on the lower, abaxial surface. Even resupinate leaves develop stomata on the lower, albeit adaxial surface (*45*), suggesting that leaf orientation (lower vs. upper) rather than leaf polarity (abaxial vs. adaxial) is causal. The covariation between stomatal density ratio and light habitat is both qualitative and quantitative. A higher proportion of sun leaves are amphistomatous (*39*) and the proportion of stomata on the upper, adaxial surface increases with light (*42*, *43*). Resolving why high light intensity favors amphistomatous dorsivental leaves is an important first step toward understanding variation in stomatal density ratio and leaf structure-function relationships more generally.

The overarching hypothesis is that leaves with greater stomatal density ratio are more common in open, sunny habitats because they increase photosynthesis most in those circumstances. An amphistomatous leaf increases photosynthetic carbon gain compared to an otherwise identical hypostomatous leaf by increasing conductance through the leaf intercellular airspaces and boundary layers; the additional water loss through a second boundary layer is typically small (*35*). We quantify this benefit as the amphistomy advantage (AA), the log-response ratio of photosynthesis in an amphistomatous leaf compared to an otherwise identical pseudohypostomatous leaf (*20*, *46*). Why would AA be greater in sun than shade? We consider three nonmutually exclusive hypotheses that we classify as ‘acclimatory’, ‘plastic’, and ‘constitutive’ (Fig. 1).

Acclimatory hypothesis: Photosynthetic induction to high light intensity typically involves increases in total leaf stomatal conductance (increased CO_2 supply), the concentration of active Rubisco, and elec-

Table 1: Three nonmutually exclusive hypotheses and directional predictions explaining why amphistomy advantage (AA) might be greater for leaves in sunny, open habitats. For each hypothesis, we make predictions for how measurement light intensity (PPFD $= 150\,\mu\text{mol}\,\text{m}^{-2}\,\text{s}^{-1}$ vs. $2000\,\mu\text{mol}\,\text{m}^{-2}\,\text{s}^{-1}$), growth light intensity (sun vs. shade), and native plant area index (PAI) would affect AA. PPFD: photosynthetic photon flux density.

Hypothesis	Measurement light intensity	Growth light intensity	Native PAI
acclimatory	$\text{AA}_{2000} > \text{AA}_{150}$	$\text{AA}_{\text{sun}} = \text{AA}_{\text{shade}}$	$\text{cor}(\text{PAI}, \text{AA}) = 0$
plastic	$\text{AA}_{2000} = \text{AA}_{150}$	$\text{AA}_{\text{sun}} > \text{AA}_{\text{shade}}$	$\text{cor}(\text{PAI}, \text{AA}) = 0$
constitutive	$\text{AA}_{2000} = \text{AA}_{150}$	$\text{AA}_{\text{sun}} = \text{AA}_{\text{shade}}$	$\text{cor}(\text{PAI}, \text{AA}) > 0$

tron transport capacity (increased CO_2 demand). A one-dimensional circuit model using the Farquhar-von Caemmerer-Berry biochemical model of C_3 photosynthesis (*47*) shows that both increased stomatal conductance and Rubisco activity should increase AA, all else being equal (Supporting Information). If the acclimatory hypothesis is correct, we predict that $\text{AA}_{2000} > \text{AA}_{150}$ for all populations regardless of native habitat or growth environment.

Plasticity hypothesis: Individuals of the same genotype often develop dramatically different leaves in sun and shade conditions (*48*). Plastic responses are likely adaptations to optimize photosynthesis at different light intensities in variable environments (*49*). Plastic changes in leaf anatomy and biochemistry could modulate AA as a byproduct. Thicker or less porous leaves, both of which are associated with high leaf mass per area (LMA), will have lower g_{ias}; leaves with increased total stomatal density and photosynthetic capacity have greater potential CO_2 supply and demand. Under the plastic hypothesis, we predict that $\text{AA}_{\text{sun}} > \text{AA}_{\text{shade}}$ for all populations and light intensities. Secondarily, AA_{sun} and $g_{\text{max,sun}}$ should also be positively associated with native light habitat if genotypes adapted to sunny, open habitats if they can express a phenotype best adapted to that environment when leaves develop under high light intensity.

Constitutive hypothesis: In environments that are relatively constant or where environmental change cannot be anticipated by a reliable cue, natural selection will favor constitutive expression of optimal phenotypes. We therefore predict genotypes from more sunny, open habitats will have consistently greater AAunder also measurement and growth light intensities. For herbaceous plants, light intensity is largely a function of the tree canopy (*50*). Herbs growing in the open will regularly experience high light intensity; herbs growing under a forest canopy will often experience low light intensity.

The primary directional predictions for each hypothesis are summarized in Table 1; detailed predictions for results that would indicate support for multiple hypotheses are in Table S6.

We tested these hypotheses by comparing AA among amphistomatous wild tomato species (*51*) from different native light habitats, grown under simulated sun and shade light treatments, and measured under contrasting light intensity (). We measured AA on 572 individual plants from 29 populations (average of 9.86 replicates per light treatment) using a recently developed method (*46*). With this method,

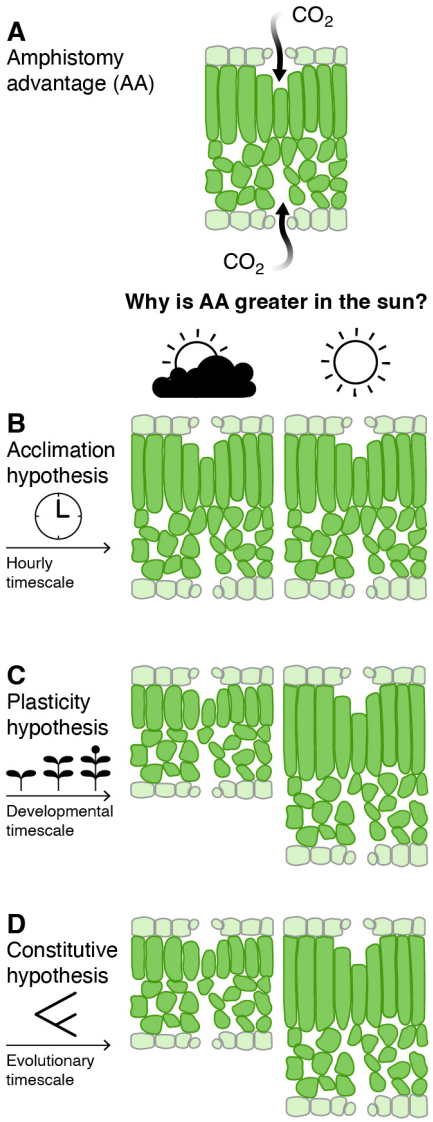

Figure 1: **Conceptual outline of three nonmutually exclusive hypotheses explaining why amphistomy advantage (AA) might be greater for leaves in sunny, open habitats.** The acclimatory hypothesis predicts that AA is greater under high measurement light intensity ($2000\,\mu mol\,m^{-2}\,s^{-1}$) than low measurement light intensity (PPFD $=$ $150\,\mu mol\,m^{-2}\,s^{-1}$), regardless of growth light intensity or native plant area index (PAI). The plasticity hypothesis predicts that AA is greater for plants grown in sun than shade, regardless of measurement light intensity or native PAI. The constitutive hypothesis predicts that AA is greater for plants adapted to sunny habitats (lower native PAI) than shaded habitats, regardless of measurement light intensity or growth light intensity.

we directly compare the photosynthetic rate of an untreated amphistomatous leaf to that of the same leaf with gas exchange blocked through the adaxial (upper) surface by transparent plastic, which we refer to as 'pseudohypostomy'. To compare amphi- and pseudohypostomatous leaves at identical whole-leaf g_{sc}, we measure A over a range of g_{sc}, inducing stomatal opening and closure by modulating humidity (see Materials and Methods for further details). We estimated 'amphistomy advantage' (AA) *sensu* (*20*), but with modifications previously described in (*46*) and here (Materials and Methods). The native light intensity was represented by plant area index (PAI $m^2\ m^{-2}$), estimated using a global gridded X-m2 resolution data set derived from the Global Ecosystem Dynamics Investigation [GEDI; (*52*)] and geo-referenced accession collection information from the Tomato Genetics Resource Center. The growth light intensities were PPFD $= 761\ \mu mol\ m^{-2}\ s^{-1}$ (sun treatment) and $115\ \mu mol\ m^{-2}\ s^{-1}$ (shade treatment) while all other environment conditions were nearly identical (see materials and methods in supplementary materials). The high and low measurements intensities were PPFD $= 2000\ \mu mol\ m^{-2}\ s^{-1}$ (97.8:2.24 red:blue) and PPFD $= 150\ \mu mol\ m^{-2}\ s^{-1}$ (87.0:13.0 red:blue), respectively.

Consistent with biophysical theory of CO_2 diffusion within leaves, AA > 0 for all populations (Fig. 2A). AA varied substantially between measurement light intensities, growth light intensities, and among populations (point to model comparison evidence). Measured under high light intensity, AA was consistently greater for sun plants. The average AA among populations in the shade treatment was 0.039 (range: 0.012–0.109; 21 of 29 populations significant); however, the same populations grown at high light intensity showed a mean AA of 0.050 (range: 0.024–0.120; 25 of 29 populations significant). Contrary to the predictions of the assimilatory hypothesis, AA was greater in all populations under low measurement light intensity for both sun and shade grown plants. The effect of low light on AA was more pronounced in the sun-grown plants, where AA was significantly greater under low measurement light intensity in 28 of 29 populations compared to to 11 populations for shade-grown plants. The overall average AA of shade and sun grown plants measured under low light intensity was 0.066 (range: 0.019–0.143; 27 of 29 populations significant) and 0.098 (range: 0.051–0.175; 29 of 29 populations significant), respectively. There was a slight tendency for populations from more closed habitats (greater PAI), but AA varied widely among populations from open habitats (low PAI) regardless of growth and measurement light intensities (Fig. 2B).

The pattern of AA across wild tomatoes strongly supports the plasticity hypothesis, argues against the acclimatory hypothesis, and provides only weak support for the constitutive hypothesis. Plastic changes in leaf thickness and/or packing density, summarized by the bulk leaf mass per area (LMA), likely mediate the effect of growth light intensity on AA. LMA increased in sun grown plants in all populations by an average of 123% [95% CI: 50.5 to 245%], similar to plastic responses in many species (*48*). When LMA is included in the model, the effect of growth light intensity on AA is no longer significant based on model comparison (Table S8) and LMA is weakly positively correlated with AA (Fig. 3). In contrast, LMA did not mediate an indirect effect of native PAI on AA (Table S8). Many anatomical traits underlie LMA (*53*) and future research will be needed identify which particular traits, such as leaf thickness or mesophyll porosity, are responsible for mediating AA. The fact that the AA of sun plants was greater under low measurement light intensity supports a long-standing hypothesis that resistance to CO_2 diffusion is greater in the upper than lower portions of the leaf interior (*54*). At low light intensity, the bulk properties of the leaf are weighed toward the upper palisade where most light is intercepted. Hence, amphistomy may, expectedly, be particularly beneficial for sun leaves

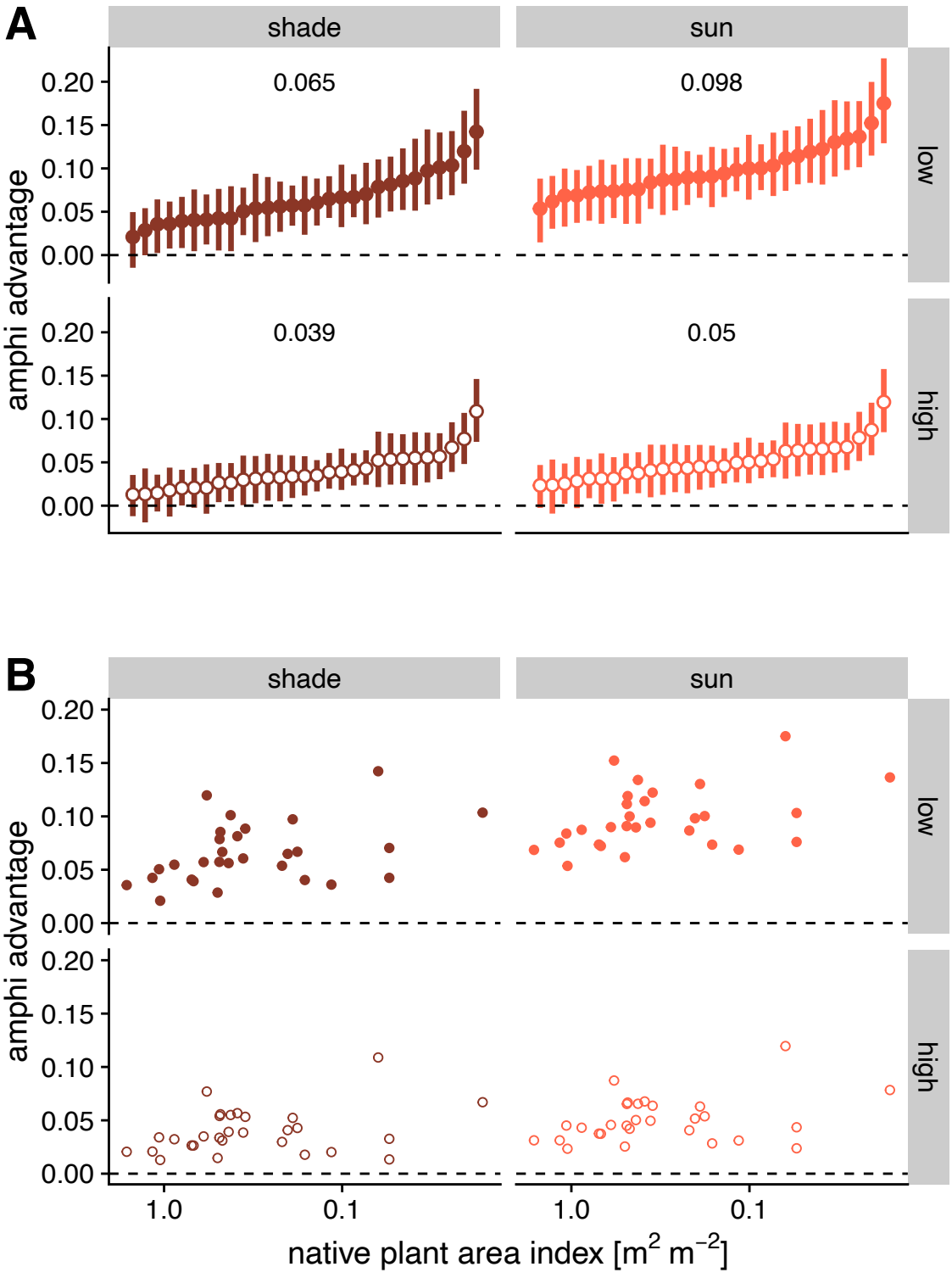

Figure 2: Caption on following page.

Figure 2: **Amphistomy advantage (**AA**) in wild tomatoes is amplified under simulated sunny growth conditions.** AA (y-axis) is the log-response ratio of photosynthesis in an amphistomatous leaf compared to an otherwise identical pseudohypostomatous leaf. In both panels, estimates are shown for plants grown under simulated shade or sun and measured under high light intensity (PPFD $= 2000\,\mu\text{mol}\,\text{m}^{-2}\,\text{s}^{-1}$) and low light intensity (PPFD $= 150\,\mu\text{mol}\,\text{m}^{-2}\,\text{s}^{-1}$). The dashed line at zero indicates no difference in photosynthesis between amphi- and pseudohypostomatous leaves. (**A**) The points are the posterior median AA for each population, with error bars showing 95% confidence intervals. Within each facet, the populations are arranged by AA estimated in that growth and measurement condition. (**B**) The same estimates of AA in each combination of growth and measurement light intensity ploted against native plant area index (PAI; x-axis, log-scale). The confidence intervals were omitted for visual clarity.

experiencing intermittant shade or cloud cover. Our study is limited in testing this because we could not directly measure the stomatal conductance ratio and intercellular resistance on each surface. Future experiments measuring AA with a dual sided chamber (*31*, *33*) can overcome these limitations.

We conclude that developmental plasticity, as opposed to acclimation or adaptation to open habitats, may explain the explain the long-standing observation that amphistomatous leaves are more common in sunny habitats, at least among herbaceous plants including crop relatives. Our results advance existing explanations by showing high light intensity *per se* does not increase the benefit of amphistomy, but rather that anatomical and biochemical change associated with higher light intensity modulate AA. Developmental plasticity needs to be considered when interpreting phylogenetic comparative analyses of adaptation, because plastic differences may be mistaken for genetic differences.

A second major conclusion is that the significant photosynthetic gain of amphistomatous leaves implies that the many hypostomatous leaves that dominate mesic to wet forests globally are giving up 'free' carbon that would require little to no additional water loss. Under realistic assumptions, we estimate that hypostomatous leaves could achieve the same A with X to X% less water loss if they were amphistomatous (Table S9). Ours is the first experimental demonstration that amphistomy is beneficial for sun leaves because of plastic changes, but future research needs to estimates the tradeoffs associated with amphistomatous leaves in order to fully explain their rarity among many woody plants and shade-tolerant herbs.

Acknowledgements

Sam McKlin and Tom Buckley helped with protocol development. Justin Alter, Max Gatlin, Joana Kim, Jenna Matsuyama, Brandon Najarian, and Kai Yasuda contributed to data collection. Sarah Friedrich helped with conceptual figure.

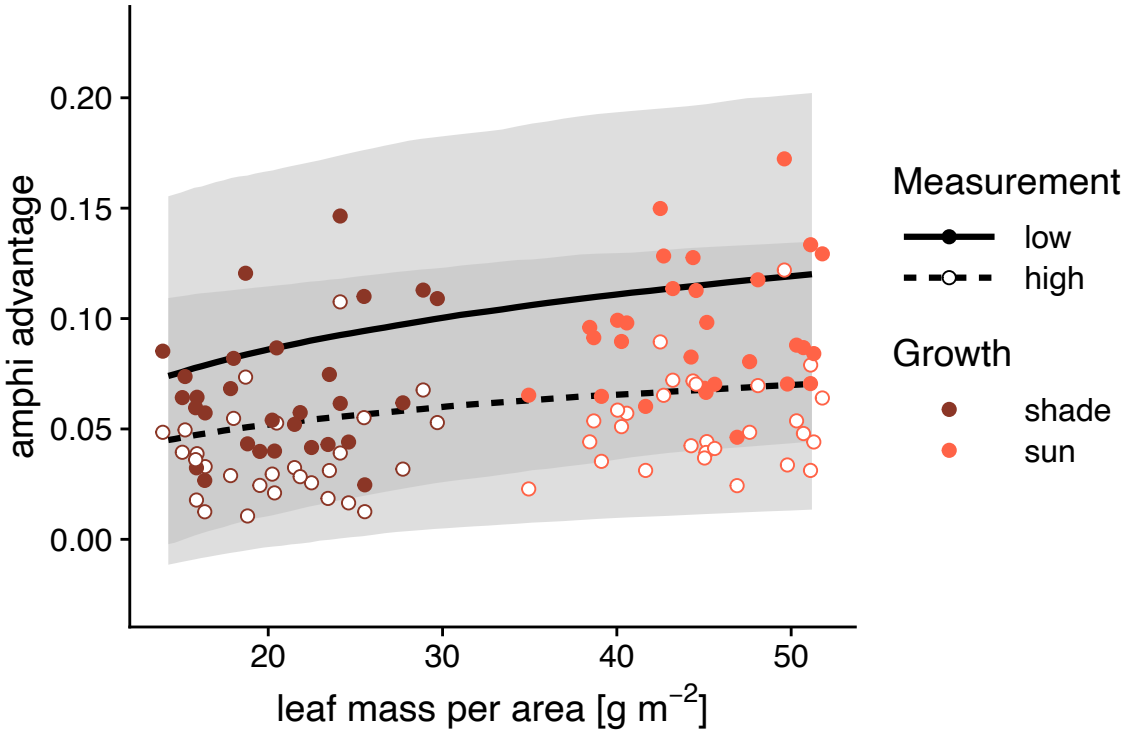

Figure 3: **Plastic changes in leaf mass per area (LMA) mediate the effect of sun- to shade-grown plants on amphistomy advantage (**AA**).** Each point is the estimated population-level LMA (x-axis) and AA (y-axis) for each population grown under high light intensity (PPFD $=$ 2000 µmol m^{-2} s^{-1}) and low light intensity (PPFD $=$ 150 µmol m^{-2} s^{-1}). The points are colored by growth light treatment. The solid line is the posterior median of the linear regression of individual-level LMA on AA_{2000} with the shaded region showing the 95% confidence ribbon; the dashed line is the same for AA_{150}. Confidence intervals for each population estimate and individual-level estimates are omitted for visual clarity.

Funding:

US National Science Foundation OIA-1929167 to C.D.M.

Author contributions:

Conceptualization: C.D.M.; Methodology: C.D.M., W.S.L.; Investigation: C.D.M., W.S.L., D.W.; Visualization: C.D.M.; Funding acquisition: C.D.M.; Writing – original draft: C.D.M.; Writing – review & editing: C.D.M., W.S.L., D.W.

References

1. J. A. Raven, Selection pressures on stomatal evolution. *New Phytologist* **153**, 371–386 (2002).

2. S. A. M. McAdam, J. G. Duckett, F. C. Sussmilch, S. Pressel, K. S. Renzaglia, R. Hedrich, T. J. Brodribb, A. Merced, Stomata: The holey grail of plant evolution. *American Journal of Botany* **108**, 366–371 (2021).

3. J. W. Clark, B. J. Harris, A. J. Hetherington, N. Hurtado-Castano, R. A. Brench, S. Casson, T. A. Williams, J. E. Gray, A. M. Hetherington, The origin and evolution of stomata. *Current Biology* **32**, R539–R553 (2022).

4. A. M. Hetherington, F. I. Woodward, The role of stomata in sensing and driving environmental change. *Nature* **424**, 901–908 (2003).

5. H. J. de Boer, C. A. Price, F. Wagner□Cremer, S. C. Dekker, P. J. Franks, E. J. Veneklaas, Optimal allocation of leaf epidermal area for gas exchange. *New Phytologist* **210**, 1219–1228 (2016).

6. E. L. Harrison, L. Arce Cubas, J. E. Gray, C. Hepworth, The influence of stomatal morphology and distribution on photosynthetic gas exchange. *The Plant Journal* **101**, 768–779 (2020).

7. F. I. Woodward, Stomatal numbers are sensitive to increases in CO2 from pre-industrial levels. *Nature* **327**, 617–618 (1987).

8. T. N. Buckley, K. A. Mott, Modelling stomatal conductance in response to environmental factors: Modelling stomatal conductance. *Plant, Cell & Environment* **36**, 1691–1699 (2013).

9. M. Haworth, C. Elliott-Kingston, J. C. McElwain, Co-ordination of physiological and morphological responses of stomata to elevated [CO2] in vascular plants. *Oecologia* **171**, 71–82 (2013).

10. X. Liang, D. Wang, Q. Ye, J. Zhang, M. Liu, H. Liu, K. Yu, Y. Wang, E. Hou, B. Zhong, L. Xu, T. Lv, S. Peng, H. Lu, P. Sicard, A. Anav, D. S. Ellsworth, Stomatal responses of terrestrial plants to global change. *Nature Communications* **14**, 2188 (2023).

11. L. C. Chua, O. S. Lau, Stomatal development in the changing climate. *Development* **151**, dev202681 (2024).

12. P. L. M. Lang, J. M. Erberich, L. Lopez, C. L. Weiß, G. Amador, H. F. Fung, S. M. Latorre, J. R. Lasky, H. A. Burbano, M. Expósito-Alonso, D. C. Bergmann, Century-long timelines of herbarium genomes predict plant stomatal response to climate change. *Nature Ecology & Evolution* **8**, 1641–1653 (2024).

13. P. J. Franks, D. L. Royer, D. J. Beerling, P. K. Van de Water, D. J. Cantrill, M. M. Barbour, J. A. Berry, New constraints on atmospheric CO_2 concentration for the Phanerozoic. *Geophysical Research Letters* **41**, 4685–4694 (2014).

14. J. C. McElwain, M. Steinthorsdottir, Paleoecology, ploidy, paleoatmospheric composition, and developmental biology: A review of the multiple uses of fossil stomata. *Plant Physiology* **174**, 650–664 (2017).

15. The Cenozoic CO Proxy Integration Project (CenCOPIP) Consortium*†, B. Hönisch, D. L. Royer, D. O. Breecker, P. J. Polissar, G. J. Bowen, M. J. Henehan, Y. Cui, M. Steinthorsdottir, J. C. McElwain, M. J. Kohn, A. Pearson, S. R. Phelps, K. T. Uno, A. Ridgwell, E. Anagnostou, J. Austermann, M. P. S. Badger, R. S. Barclay, P. K. Bijl, T. B. Chalk, C. R. Scotese, E. De La Vega, R. M. DeConto, K. A. Dyez, V. Ferrini, P. J. Franks, C. F. Giulivi, M. Gutjahr, D. T. Harper, L. L. Haynes, M. Huber, K. E. Snell, B. A. Keisling, W. Konrad, T. K. Lowenstein, A. Malinverno, M. Guillermic, L. M. Mejía, J. N. Milligan, J. J. Morton, L. Nordt, R. Whiteford, A. Roth-Nebelsick, J. K. C. Rugenstein, M. F. Schaller, N. D. Sheldon, S. Sosdian, E. B. Wilkes, C. R. Witkowski, Y. G. Zhang, L. Anderson, D. J. Beerling, C. Bolton, T. E. Cerling, J. M. Cotton, J. Da, D. D. Ekart, G. L. Foster, D. R. Greenwood, E. G. Hyland, E. A. Jagniecki, J. P. Jasper, J. B. Kowalczyk, L. Kunzmann, W. M. Kürschner, C. E. Lawrence, C. H. Lear, M. A. Martínez-Botí, D. P. Maxbauer, P. Montagna, B. D. A. Naafs, J. W. B. Rae, M. Raitzsch, G. J. Retallack, S. J. Ring, O. Seki, J. Sepúlveda, A. Sinha, T. F. Tesfamichael, A. Tripati, J. Van Der Burgh, J. Yu, J. C. Zachos, L. Zhang, Toward a Cenozoic history of atmospheric CO_2. *Science* **382**, eadi5177 (2023).

16. T. A. Hofmann, W. Atkinson, M. Fan, A. J. Simkin, P. Jindal, T. Lawson, Impact of climate-driven changes in temperature on stomatal anatomy and physiology. *Philosophical Transactions of the Royal Society B: Biological Sciences* **380**, 20240244 (2025).

17. J. A. Berry, D. J. Beerling, P. J. Franks, Stomata: Key players in the earth system, past and present. *Current Opinion in Plant Biology* **13**, 232–239 (2010).

18. P. J. Franks, J. A. Berry, D. L. Lombardozzi, G. B. Bonan, Stomatal Function across Temporal and Spatial Scales: Deep-Time Trends, Land-Atmosphere Coupling and Global Models. *Plant Physiology* **174**, 583–602 (2017).

19. P. J. Grubb, "Leaf structure and function" in *The Encyclopedia of Ignorance*, R. Duncan, M. Weston-Smith, Eds. (Pergamon, Oxford, 1977)vol. 2, pp. 317–330.

20. D. F. Parkhurst, The adaptive significance of stomatal occurrence on one or both surfaces of leaves. *The Journal of Ecology* **66**, 367–383 (1978).

21. K. A. Mott, A. C. Gibson, J. W. O'Leary, The adaptive significance of amphistomatic leaves. *Plant, Cell & Environment* **5**, 455–460 (1982).

22. A. C. Gibson, *Structure-Function Relations of Warm Desert Plants* (Springer Berlin / Heidelberg, Berlin, Heidelberg, 1996; http://public.eblib.com/choice/PublicFullRecord.aspx?p=6495247).

23. W. K. Smith, T. C. Vogelmann, E. H. DeLucia, D. T. Bell, K. A. Shepherd, Leaf Form and Photosynthesis. *BioScience* **47**, 785–793 (1997).

24. R. Oguchi, Y. Onoda, I. Terashima, D. Tholen, "Leaf Anatomy and Function" in *The Leaf: A Platform for Performing Photosynthesis*, W. W. Adams III, I. Terashima, Eds. (Springer International Publishing, Cham, 2018; https://doi.org/10.1007/978-3-319-93594-2_5)*Advances in Photosynthesis and Respiration*, pp. 97–139.

25. P. L. Drake, H. J. de Boer, S. J. Schymanski, E. J. Veneklaas, Two sides to every leaf: Water and CO_2 transport in hypostomatous and amphistomatous leaves. *New Phytologist* **222**, 1179–1187 (2019).

26. P. J. Grubb, "Leaf structure and function" in *Unsolved Problems in Ecology*, A. Dobson, D. Tilman, R. D. Holt, Eds. (Princeton University Press, Princeton, 2020), pp. 124–144.

27. J. Pospíšilová, J. Solárová, Environmental and biological control of diffusive conductances of adaxial and abaxial leaf epidermes. *Photosynthetica* **14**, 90–127 (1980).

28. K. A. Mott, J. W. O'Leary, Stomatal Behavior and CO□ Exchange Characteristics in Amphistomatous Leaves. *Plant Physiology* **74**, 47–51 (1984).

29. P. B. Reich, A. W. Schoettle, R. G. Amundson, Effects of low concentrations of O3, leaf age and water stress on leaf diffusive conductance and water use efficiency in soybean. *Physiologia Plantarum* **63**, 58–64 (1985).

30. K. A. Mott, Z. G. Cardon, J. A. Berry, Asymmetric patchy stomatal closure for the two surfaces of *Xanthium strumarium* L. Leaves at low humidity. *Plant, Cell & Environment* **16**, 25–34 (1993).

31. S. Wall, S. Vialet□Chabrand, P. Davey, J. Van Rie, A. Galle, J. Cockram, T. Lawson, Stomata on the abaxial and adaxial leaf surfaces contribute differently to leaf gas exchange and photosynthesis in wheat. *New Phytologist* **235**, 1743–1756 (2022).

32. V. P. Gutschick, Photosynthesis model for C_3 leaves incorporating CO_2 transport, propagation of radiation, and biochemistry 2. Ecological and agricultural utility. *Photosynthetica* **18**, 569–595 (1984).

33. D. A. Márquez, H. Stuart□Williams, L. A. Cernusak, G. D. Farquhar, Assessing the CO_2 concentration at the surface of photosynthetic mesophyll cells. *New Phytologist* **238**, 1446–1460 (2023).

34. D. F. Parkhurst, K. A. Mott, Intercellular diffusion limits to CO_2 uptake in leaves: Studies in air and helox. *Plant Physiology* **94**, 1024–1032 (1990).

35. J. R. Foster, W. K. Smith, Influence of stomatal distribution on transpiration in low-wind environments. *Plant, Cell and Environment* **9**, 751–759 (1986).

36. C. D. Muir, Is amphistomy an adaptation to high light? Optimality models of stomatal traits along light gradients. *Integrative and Comparative Biology* **59**, 571–584 (2019).

37. J. G. Wood, The physiology of xerophytism in Australian plants: The stomatal frequencies, transpiration and osmotic pressures of sclerophyll and tomentose-succulent leaved plants. *Journal of Ecology* **22**, 69–87 (1934).

38. J. T. Howell, Concerning stomata on leaves in *a*rctostaphylos. *The Wasmann Collector* **6**, 57–65 (1945).

39. E. J. Salisbury, I. On the causes and ecological significance of stomatal frequency, with special reference to the woodland flora. *Philosophical Transactions of the Royal Society of London. Series B, Containing Papers of a Biological Character* **216**, 1–65 (1928).

40. H. J. Peat, A. H. Fitter, A comparative study of the distribution and density of stomata in the British flora. *Biological Journal of the Linnean Society* **52**, 377–393 (1994).

41. G. J. Jordan, R. J. Carpenter, T. J. Brodribb, Using fossil leaves as evidence for open vegetation. *Palaeogeography, Palaeoclimatology, Palaeoecology* **395**, 168–175 (2014).

42. S. F. Bucher, K. Auerswald, C. Grün-Wenzel, S. I. Higgins, J. Garcia Jorge, C. Römermann, Stomatal traits relate to habitat preferences of herbaceous species in a temperate climate. *Flora* **229**, 107–115 (2017).

43. C. D. Muir, Light and growth form interact to shape stomatal ratio among British angiosperms. *New Phytologist* **218**, 242–252 (2018).

44. G. Triplett, A. S. David, Stomatal distribution and post□fire recovery: Intra□ and interspecific variation in plants of the pyrogenic Florida scrub. *American Journal of Botany*, e70050 (2025).

45. O. B. Lyshede, Comparative and functional leaf anatomy of selected Alstroemeriaceae of mainly Chilean origin. *Botanical Journal of the Linnean Society* **140**, 261–272 (2002).

46. G. Triplett, T. N. Buckley, C. D. Muir, Amphistomy increases leaf photosynthesis more in coastal than montane plants of Hawaiian ʻilima (*Sida fallax*). *American Journal of Botany* **111**, e16284 (2024).

47. G. D. Farquhar, S. von Caemmerer, J. A. Berry, A biochemical model of photosynthetic CO_2 assimilation in leaves of C_3 species. *Planta* **149**, 78–90 (1980).

48. H. Poorter, Ü. Niinemets, N. Ntagkas, A. Siebenkäs, M. Mäenpää, S. Matsubara, T. L. Pons, A meta□analysis of plant responses to light intensity for 70 traits ranging from molecules to whole plant performance. *New Phytologist* **223**, 1073–1105 (2019).

49. T. J. Givnish, R. A. Montgomery, Common-garden studies on adaptive radiation of photosynthetic physiology among Hawaiian lobeliads. *Proceedings of the Royal Society B: Biological Sciences* **281**, 20132944–20132944 (2014).

50. B. M. J. Engelbrecht, H. M. Herz, Evaluation of different methods to estimate understorey light conditions in tropical forests. *Journal of Tropical Ecology* **17**, 207–224 (2001).

51. I. E. Peralta, D. M. Spooner, S. Knapp, Taxonomy of wild tomatoes and their relatives (*solanum* sect. *Lycopersicoides*, sect. *Juglandifolia*, sect. *Lycopersicon*; Solanaceae). **84** (2008).

52. P. Burns, C. R. Hakkenberg, S. J. Goetz, Multi-resolution gridded maps of vegetation structure from GEDI. *Scientific Data* **11**, 881 (2024).

53. G. P. John, C. Scoffoni, T. N. Buckley, R. Villar, H. Poorter, L. Sack, The anatomical and compositional basis of leaf mass per area. *Ecology Letters* **20**, 412–425 (2017).

54. H. G. Jones, R. O. Slatyer, Effects of Intercellular Resistances on Estimates of the Intracellular Resistance to Co2 Uptake by Plant Leaves. *Australian Journal of Biological Sciences* **25**, 443 (1972).

55. P.-G. Schoch, C. Zinsou, M. Sibi, Dependence of the stomatal index on environmental factors during stomatal differentiation in leaves of *Vigna sinensis* L.: 1. Effect of light intensity. *Journal of Experimental Botany* **31**, 1211–1216 (1980).

56. L. Sack, T. N. Buckley, The developmental basis of stomatal density and flux. *Plant Physiology* **171**, 2358–2363 (2016).

57. K. A. Mott, O. Michaelson, Amphistomy as an adaptation to high light intensity in *Ambrosia cordifolia* (Compositae). *American Journal of Botany* **78**, 76–79 (1991).

58. J. Schindelin, I. Arganda-Carreras, E. Frise, V. Kaynig, M. Longair, T. Pietzsch, S. Preibisch, C. Rueden, S. Saalfeld, B. Schmid, J.-Y. Tinevez, D. J. White, V. Hartenstein, K. Eliceiri, P. Tomancak, A. Cardona, Fiji: An open-source platform for biological-image analysis. *Nature Methods* **9**, 676–682 (2012).

59. B. Marshall, P. V. Biscoe, A Model for C_3 Leaves Describing the Dependence of Net Photosynthesis on Irradiance. *Journal of Experimental Botany* **31**, 29–39 (1980).

60. T. V. Elzhov, K. M. Mullen, A.-N. Spiess, B. M. Bolker, *Minpack.lm: R Interface to the Levenberg-Marquardt Nonlinear Least-Squares Algorithm Found in MINPACK, Plus Support for Bounds* (2023; https://CRAN.R-project.org/package=minpack.lm).

61. Stan Development Team, *Stan Modeling Language Users Guide and Reference Manual* (2025; https://mc-stan.org).

62. P.-C. Bürkner, **Brms** : An *r* Package for Bayesian Multilevel Models Using *stan*. *Journal of Statistical Software* **80** (2017).

63. J. Gabry, R. Češnovar, A. Johnson, S. Bronder, *Cmdstanr: R Interface to 'CmdStan'* (2025; https://mc-stan.org/cmdstanr, https://discourse.mc-stan.org).

64. R Core Team, *R: A Language and Environment for Statistical Computing* (R Foundation for Statistical Computing, Vienna, Austria, 2025; http://www.R-project.org/).

65. A. Gelman, D. B. Rubin, Inference from iterative simulation using multiple sequences. *Statistical Science* **7**, 457–472 (1992).

66. T. F. Hansen, Stabilizing selection and the comparative analysis of adaptation. *Evolution* **51**, 1341–1351 (1997).

67. A. Vehtari, A. Gelman, J. Gabry, Practical Bayesian model evaluation using leave-one-out cross-validation and WAIC. *Statistics and Computing* **27**, 1413–1432 (2017).

Supplementary Materials

Materials and Methods

Populations

We compared AA among 29 ecologically diverse populations of wild tomato, including representatives of all described species of *Solanum* sect. *Lycopersicon* and sect. *Lycopersicoides* (*51*) and the cultivated tomato *S. lycopersicum* var. *lycopersicum* (Table S1). Due to constraints on growth space and time, we spread out measurements over 61.1 weeks from August 29, 2022 to October 31, 2023. Replicates within population were evenly spread out over this period to prevent confounding of temporal variation in growth conditions with accession. [anything else to say here? maybe explain population selection and phylogeny?]

Table S1: Accession information of *Solanum* populations used in this study. The species name, accession number, collection latitude, longitude, elevation, and daily solar radiation estimated using the SPLASH algorithm (see 'Climate data'). TGRC: Tomato Genetics Resource Center; PAI: Plant area index.

Species	TGRC accession	Latitude	Longitude	Elevation (mas)	PAI ($m^2\ m^{-2}$)
S. arcanum	LA2172	-6.008	-78.858	662	0.70
S. cheesmaniae	LA0429	-0.644	-90.329	800	0.60
S. cheesmaniae	LA3124	-0.804	-90.042	1	0.36
S. chilense	LA1782	-15.267	-74.633	1000	0.35
S. chilense	LA4117A	-22.907	-67.941	3540	0.22
S. chmielewskii	LA1028	-13.883	-73.017	3000	0.43
S. chmielewskii	LA1316	-13.400	-73.906	2920	1.07
S. corneliomulleri	LA0107	-13.117	-76.383	60	0.02
S. corneliomulleri	LA0444	-13.433	-76.133	100	0.49
S. galapagense	LA0436	-0.953	-90.978	40	0.20
S. galapagense	LA1044	-0.284	-90.548	0	0.18
S. habrochaites	LA0407	-2.181	-79.884	70	0.47
S. habrochaites	LA1777	-9.550	-77.700	3216	0.42
S. huaylasense	LA1358	-9.533	-77.967	750	0.58
S. huaylasense	LA1360	-9.546	-77.929	1490	0.48
S. huaylasense	LA1364	-10.133	-77.383	2920	0.88
S. lycopersicoides	LA2951	-19.317	-69.450	2200	0.49
S. lycopersicoides	LA4126	-19.287	-69.396	3120	0.39
S. neorickii	LA1322	-13.483	-72.442	2380	0.68
S. neorickii	LA2133	-3.400	-79.183	1980	1.05

S. pennellii	LA0716	-16.225	-73.617	50	0.19
S. pennellii	LA0750	-14.775	-75.034	550	0.05
S. pennellii	LA3778	-14.775	-75.034	616	0.05
S. peruvianum	LA2744	-18.550	-70.150	400	0.16
S. peruvianum	LA2964	-18.028	-70.835	75	1.16
S. pimpinellifolium	LA1269	-11.483	-77.075	400	0.50
S. pimpinellifolium	LA1589	-8.433	-78.817	30	0.11
S. pimpinellifolium	LA2933	-1.442	-80.562	375	1.62
S. sitiens	LA4116	-22.159	-68.782	2960	0.06

Plant growth conditions

In all growth spaces, we recorded PPFD using full spectrum quantum sensors (SQ-500-SS, Apogee Instruments, Logan, Utah, USA); we recorded temperature, RH, and $[CO_2]$ using an EE894 sensor (E+E Elektronik, Engerwitzdorf, Austria) protected by a radiation shield. All environmental measurements were taken every 10 minutes from the middle of plants racks at approximately the same height as the leaves we measured. We measured leaf temperature of focal leaves prior to measurement using an infrared radiometer (SI-111-SS, Apogee Instruments, Logan, Utah, USA).

Germination and seedling stage

Seeds provided by the Tomato Genetics Resource Center germinated on moist paper in plastic boxes after soaking for 30-60 minutes in a 50% (volume per volume) solution of household bleach and water, followed by a thorough rinse. We transferred seedlings to cell-pack flats containing Pro-Mix BX potting mix (Premier Tech, Rivière-du-Loup, Quebec, Canada) once cotyledons fully emerged, typically within 1-2 weeks of sowing. We grew seeds and seedlings for both sun and shade treatments under the same environmental conditions (12:12 h, 24.3:21.7 °C, 49.6:58.4 RH day:night cycle). LED light provided PPFD $= 267\ \mu mol\ m^{-2}\ s^{-1}$ (Fluence RAZRx, Austin, Texas, USA).

Light treatments

Seedlings were randomly assigned in alternating order within population to the sun or shade treatment during transplanting. After seedlings established in cell-pack flats for $\approx$ 2 weeks, we transplanted them to 3.78 L plastic pots containing 60% Pro-Mix BX potting mix, 20% coral sand (Pro-Pak, Honolulu, Hawai‘i, USA), and 20% cinders (Niu Nursery, Honolulu, Hawai‘i, USA). Percentage composition is on a volume basis. The soil mixture contained slow release NPK fertilizer following manufacturer instructions (Osmocote Smart-Release Plant Food Flower & Vegetable, The Scotts Company, Marysville, Ohio, USA). We determined pot field capacity one week after transplanting using a scale (Ohaus V12P15 Valor 1000, Parsippany, New Jersey, USA) and watered to field capacity three times per week to prevent drought stress.

We assigned sun and shade treatment to lower and upper racks of a $1.22\,\mathrm{m} \times 2.44\,\mathrm{m}$ shelving unit in a climate-controlled growth room. We assigned the sun treatment to the lower rack to limit diffuse light from reaching the shade treatment. The average daytime PPFD was $761\,\mu\mathrm{mol\,m^{-2}\,s^{-1}}$ and $115\,\mu\mathrm{mol\,m^{-2}\,s^{-1}}$ for sun and shade treatments, respectively. To isolate the effect of light intensity from quality, we used the same LED model with the the same spectrum (Fluence SPYDR 2i, Austin, Texas, USAS), but dimmed the lights in the shade treatment. To maintain homogeneous environmental conditions other than light, we mixed air within the growth room using an air circulator (Vornado 693DC, Andover, Kansas, USA) and within racks using a miniature oscillating air circulator (Vornado Atom 1, Andover, Kansas, USA). Despite these efforts, the air in the sun treatment was on average $2.56\,°\mathrm{C}$ warmer and the average RH was consequently 5.75% lower. However, because of evaporative cooling, the leaves in the sun treatment were only $0.886\,°\mathrm{C}$ on average ($n = 699$ leaves).

Leaf trait measurements

We selected a fully expanded, unshaded leaf at least six leaves above the cotyledons during early vegetative growth. This typically meant that plants had grown in light treatments for ≈ 4 weeks, ensuring they had time to sense and respond developmentally to the light intensity of the treatment rather than the seedling conditions (*55*). Shade plants grew slower than sun plants, hence leaves at the same developmental stage were measured on chronologically older plants in the shade treatment. In some sun plants, we had to use leaves higher on the stem because short internodes made lower leaves inaccessible with the gas exchange equipment. We measured terminal leaflets in 82.6% of cases, but used the lateral leaflet closest to the terminal leaflet when it was damaged or difficult to clamp into the gas exchange chamber. When a leaflet was damaged during gas exchange measurements, we collected anatomical data from the nearest leaflet on the same leaf (1.58)%. We measured chlorophyll concentration index (CCI) using a chrolophyll concentration meter (MC-100, Apogee Instruments, Logan, Utah, USA) on the lamina of focal leaflets before gas exchange measurements at the same time we measured leaf temperature.

Amphistomy advantage

We estimated 'amphistomy advantage' (AA) *sensu* (*20*), but with modifications previously described in (*46*). AA is calculated as the log-response ratio of A compared at the same total g_{sw}:

$$\mathrm{AA} = \log(A_{\mathrm{amphi}}/A_{\mathrm{hypo}})$$

We measured the photosynthetic rate of an untreated amphistomatous leaf (A_{amphi}) over a range of g_{sw} values. We refer to this as an A–g_{sw} curve. We compared the A–g_{sw} curve of the untreated leaf to the photosynthetic rate of pseudohypostomatous leaf (A_{hypo}), which is the same leaf but with gas exchange through the upper surface blocked by a neutral density plastic (propafilm).

We measured A–g_{sw} curves using a portable infrared gas analyzer (LI-6800PF, LI-COR Biosciences, Lincoln, Nebraska, USA). Light-acclimated plants were placed under LEDs dimmed to match their light

treatment during gas exchange measurements. We estimated the photosynthetic rate (A) and stomatal conductance to CO_2 (g_{sw}) at ambient CO_2 ($C_a = 415\,\mu mol\,mol^{-1}$) and $T_{leaf} = 25.0\,°C$. The irradiance of the light source in the pseudohypo leaf was higher because the propafilm reduces transmission. To compensate for reduced transmission, we increased incident PPFDfor pseudohypo leaves by a factor 1/0.91, the inverse of the measured transmissivity of the propafilm. We also set the stomatal conductance ratio, for purposes of calculating boundary layer conductance, to 0 for pseudohypo leaves following manufacturer directions.

We collected four A–g_{sw} curves per leaf, an amphi (untreated) curve and a pseudohypo (treated) curve at high light-intensity (PPFD $= 2000\,\mu mol\,m^{-2}\,s^{-1}$; 97.8:2.24 red:blue) and low light-intensity (PPFD $= 150\,\mu mol\,m^{-2}\,s^{-1}$; 87.0:13.0 red:blue). We always measured high light-intensity curves first because photosynthetic downregulation is faster than upregulation in these species. To control for order effects, we alternated between starting with amphi or pseudohypo leaf measurements. Unlike (*46*), preliminary experiments with *Solanum* indicated a strong order effect in that A declined in the second curve. Therefore, we made measurements over two days. On the first day, we measured high and low light-intensity curves for either amphi or pseudohypo leaves; on the second day, we measured high and low light-intensity curves on the other leaf type.

In all cases, we acclimated the focal leaf to high light (PPFD $= 2000\,\mu mol\,m^{-2}\,s^{-1}$) and high relative humidity (RH $= 70\%$) until A and g_{sw} reach their maximum. After that, we decreased RH to $\approx 10\%$ to induce rapid stomatal closure without biochemical downregulation. Hence, A_{amphi} and A_{hypo} were both measured at low chamber humidity after the leaf had acclimated to high humidity. All other environmental conditions in the leaf chamber remained the same. We logged data until g_{sw} reached its nadir. We then acclimated the leaf to low light (PPFD $= 150\,\mu mol\,m^{-2}\,s^{-1}$) and RH $= 70\%$ before inducing stomatal closure with low RHand logging data as described above.

Light-response (A–Q) curves

In 91.3% of plants, we measured light-response (A–Q) curves on the same leaflets as A–g_{sw} curves. However, when a leaflet was damaged during A–g_{sw} curves, we used the next closest leaflet for A–Q curves. Leaves acclimated to high light-intensity (PPFD $= 2000\,\mu mol\,m^{-2}\,s^{-1}$), ambient CO_2 ($C_a = 415\,\mu mol\,mol^{-1}$), RH $= 50\%$, and $T_{leaf} = 25\,°C$. After A and g_{sw} stabilized, we measured A at 20 light-intensity levels between 0 and $2000\,\mu mol\,m^{-2}\,s^{-1}$ in descending order.

Stomatal anatomy

We estimated the stomatal density and size on ab- and adaxial leaf surfaces from all leaves, using guard cell length as a proxy for stomatal size since it proportional to maximum conductance (*56*). We made surface impressions of leaf lamina from the same area used for gas exchange measurements using a-silicone impression material (Zhermack elite HD+, light body, fast set, Rovigo, Italy). We applied clear nail polish to make positive replicas of the impression. After nail polish dried, we mounted replicas on a microscope slide using transparent tape (*57*). We digitized a portion of each leaf surface replica using a brightfield microscope (Leica DM2000, Wetzlar, Germany). We counted and measured guard

Table S2: Six sequential steps for cleaning A–g_{sw} curves. The rationale and procedure for each step are described in the text. The rightmost columns summarize the number of curves and mean number of points per curve remaining after each step. For reference, there are four possible A–g_{sw} curves per replicate: all combinations of leaf type (amphi or pseudohypo) and light intensity (high or low).

Step: description	Number of curves	Number of points per curve
1. remove unreliable and unusable data points	2,361	63.0
2. remove hysteretic portion of A–g_{sw} curves at low g_{sw}	2,360	59.2
3. remove outliers within each A–g_{sw} curve	2,360	58.7
4. remove replicates with no overlap between amphi and pseudohypo A–g_{sw} curves	2,268	58.5
5. thin redundant data points within each A–g_{sw} curve	2,268	28.1
6. trim extreme AA values	2,214	28.1

cell length on all stomata using the FIJI implementation of ImageJ2 version 2.3.0 (*58*), then divided the count by the visible leaf area ($0.890\,\text{mm}^2$) to estimate stomatal density.

Leaf mass per area

Leaf mass per area (LMA) is the dry mass divided by the leaflet area. We scanned fresh leaflets on a flat bed scanner (Epson V600, Los Alamitos, California. USA) and measured leaflet area from digital images using the FIJI implementation of ImageJ2 version 2.3.0 (*58*). We dried leaves for 72 hours at $74\,°\text{C}$ in a food dehydrator (Cosori CP267-FD, Vesync Co., Anaheim, California, USA) and weighed using a benchtop analytical balance (Ohaus PR64 Analytical Balance, Parsippany, New Jersey, USA). In 10.5% we measured LMA on the adjacent leaflet because the focal leaflet was damaged or wilted while making surface impressions and we could not reliably estimate area. LMA data are missing from 2.97% of individuals because the area or mass was not recorded at all or recorded incorrectly.

Cleaning A–g_{sw} curves

The raw data set consisted of 2,370 A–g_{sw} curves with an average of 63.2 points per curve. Manual curation of a data set this size in a principled, consistent manner is not feasible. Therefore, we automated data cleaning using custom *R* scripts. Cleaning is divided into six sequential steps (Table S2).

Remove unreliable and unusable data points

Rationale: Unreliable data points consisted of those where chamber [CO_2] was unstable and therefore measurements are not biologically meaningful. Unusable data points were those where $A < 0$ because the logarithm of a negative number is undefined.

Procedure: We retained data points where $410 < C_a < 420\ \mu mol\ mol^{-1}$ and $A > 0$.

Remove hysteretic portion of A–g_{sw} curves at low g_{sw}

Rationale: In most A–g_{sw} curves, we observed a hysteretic response at low g_{sw}. After g_{sw} and A declined simultaneously, A increased slightly as g_{sw} continued to decline or stabilize, indicating some leaf acclimation to low RH. We removed this portion of the curve to focus curve-fitting on the primary domain where A increases monotonically with g_{sw}.

Procedure: For each curve, we removed data points after g_{sw} had reached its minimum unless there were fewer than 10 data points remaining.

Remove outliers within each A–g_{sw} curve

Rationale: Individual outliers within A–g_{sw} curves, usually caused by transitory changes in chamber conditions, exert undue leverage on parameter estimates and cause bias and/or low precision in parameter estimates.

Procedure: We fit provisional quadratic regressions for each curve using ordinary least squares with the `lm()` function in *R*. We sequentially removed data points with an absolute external studentized residual > 3 until none remained.

Thin redundant data points within each A–g_{sw} curve

Rationale: Data points closely spaced along the A–g_{sw} curve provide redundant information and may be highly correlated (i.e. pseudoreplication). This occurred because data was logged at a constant temporal interval, but the rate at which g_{sw} declined was not constant. Thinning reduces parameter estimation bias toward densely sampled regions of the curve which may not be the most biologically informative.

Procedure: We retained the maxima and minima g_{sw} for each curve and thinned all but one point per thinning interval of $0.05\ \log(mol\ m^{-2}\ s^{-1})$, retaining the point nearest the midpoint of the interval.

Remove replicates with no overlap between amphi and pseudohypo A–g_{sw} curves

Rationale: We could not estimate AA for replicates where amphi and pseudohypo A–g_{sw} curves did not overlap.

Procedure: We removed replicates where the range of g_{sw} values for amphi and pseudohypo A–g_{sw} curves did not overlap.

Table S3: Two sequential steps for cleaning A–g_{sw} curves. The rationale and procedure for each step are described in the text. The rightmost columns summarize the number of curves and mean number of points per curve remaining after each step.

Step: description	Number of curves	Number of points per curve
1. remove outliers within each A–Q curve	658	19.1
2. remove A–Q curves with poor fit	652	19.1

Trim extreme AA values

Rationale: Extreme AA values were likely due to measurement error or leaf damage. Since amphi and pseudohypo A–g_{sw} curves are measured on consecutive days, a poor calibration or a damaged leaf could cause a large difference in A between days, which would appear as an extreme AA value.

Procedure: We provionsally estimated AA for each replicate by integrating over the range of g_{sw} values where amphi and pseudohypo A–g_{sw} curves overlap. In this procedure, curve parameters were provisionally estimated using ordinary least squares with the `lm()` function in *R*. We then used point estimates of AA for each replicate as the response variable in a linear model with light treatment, light intensity, population, and all interactions as explanatory variables. This model was also fit using ordinary least squares with the `lm()` function in *R*. We classified extreme AA values as those with an absolute internal studentized residual > 3. Because these values likely indicate significant measurement error or leaf damage, we removed A–g_{sw} curves at both light intensities if either was classified as extreme.

Cleaning A–Q curves

The raw data set consisted of 658 A–Q curves with an average of 19.4. Manual curation of a data set this size in a principled, consistent manner is not feasible. Therefore, we automated data cleaning using custom *R* scripts. Cleaning is divided into two sequential steps (Table S3).

Remove outliers within each A–Q curve

Rationale: Individual outliers within A–g_{sw} curves, usually caused by transitory changes in chamber conditions, exert undue leverage on parameter estimates and cause bias and/or low precision in parameter estimates.

Procedure: We fit provisional nonrectangular hyperbola (*59*) to each A–Q curve using nonlinear regression with the `nlsLM()` function from the *R* package **minpack.lm** version 1.2.4 (*60*). We sequentially removed data points with an absolute external studentized residual > 3 until none remained.

Table S4: Summary of differences among competing models of how AA varies with light intensity, light treatment, and among populations as a function of native PPFD. The models are numbered from simpler to more complex. All models include fixed effects of light intensity and light treatment; some models include interactions between. All models include a phylogenetic random effect of population on AA; some models include varying effects of light intensity and light treatment among populations. The last column indicates the population-level AA variable we used as a response to native PPFD.

Model	Fixed effects	Phylogenetic random effects	Response to native PPFD
1	light intensity light treatment	varying intercept among populations	$AA_{0,acc}$
2	light intensity light treatment intensity $\times$ treatment	varying intercept among populations	$AA_{0,acc}$
3	light intensity light treatment	varying intercept among populations varying effect of high light intensity among populations	$AA_{2000,acc}$
4	light intensity light treatment	varying intercept among populations varying effect of sun treatment among populations	$AA_{sun,\ acc}$
5	light intensity light treatment intensity $\times$ treatment	varying intercept among populations varying effect of high light intensity among populations varying effect of sun treatment among populations	$AA_{2000,sun,\ acc}$

Remove A–Q curves with poor fit

Rationale: A–Q curves with a poor fit to the nonrectangular hyperbola most likely indicate systematic measurement error and/or the leaf was not fully acclimated to the chamber environment.

Procedure: As described above, we fit provisional nonrectangular hyperbola to each A–Q curve and calculated the model r^2. There was a clear break between typical curves and poorly fitting curves where $r^2 < 0.99$. We therefore removed A–Q curves with $r^2 < 0.99$.

Bayesian data analysis in *Stan*

We fit five models to test predictions of competing hypotheses about why amphistomy advantage (AA) might be greater for leaves in sunny, open habitats. This section provides an overview of differences among models (Table S4). The next sections describe how we fit models in *Stan*, all model parameters and priors, and specific predictions about parameter values for each hypothesis.

Fitting models in *Stan*

We fit Bayesian models with MCMC sampling in the probabilistic programming language *Stan* (*61*) using the *R* package **brms** version 2.22.0 (*62*). We used *CmdStan* version 2.35.0 and **cmdstanr** version 0.9.0 (*63*) to interface with *R* version 4.5.0 (*64*). We sampled the posterior distribution from 1 chains with 2000 iterations each after 2000 warmup iterations per chain. We estimated parameters and confidence intervals as the median and 95% quantile intervals of the posterior, respectively. We chose the number of chains, warmup and sampling iterations, and maximum treedepth so that parameter estimates converged ($\widehat{R} < 1.01$ (*65*)) and the effective sample size (ESS) for each parameter was > 400.

Parameter estimation and priors

There were four levels of parameter estimation in our analysis:

1. Estimate A–g_{sw} curve parameters
2. Estimate AA for each light intensity with leaf using A–g_{sw} curve parameters
3. Estimate the effects of light intensity, light treatment, and population on AA (assimilatory and plasticity hypotheses)
4. Estimate the effects of native light habitat on population-level AA (constitutive hypothesis)

Although the higher-level parameter estimates depend on the lower-level parameter estimates, we fit all models simultaneously to ensure that the uncertainty in lower-level estimates propagated to higher-level estimates.

Table S5: Description of parameters estimated in the hierarchical Bayesian model. The `Parameter` column lists the parameter name as it appears in text. The `Description` column provides a brief description of the parameter.

Parameter	Description
A–g_{sw} **curve parameters**	
$\mathbf{B}_{\text{curve}}$	$n_{\text{curve}} \times 3$ array of random A–g_{sw} curve-level coefficients ($b_{0,j}$, $b_{1,j}$, $b_{2,j}$); $\mathbf{B}_{\text{curve}} \sim \text{MVN}(\vec{0}, \mathbf{\Sigma}_{\text{curve}})$
$\vec{\beta}_{\text{curve}}$	vector of mean quadratic coefficients (β_0, β_1, β_2)
$\mathbf{\Sigma}_{\text{curve}}$	3×3 covariance matrix of curve-level coefficients
$\sigma_{6\,\text{cm}^2,\epsilon}$	minimum residual standard deviation when the measured leaf surface area is 6 cm^2
$\beta_{S,\epsilon}$	slope of the relationship between residual standard deviation and measured leaf surface area (log-link scale)
ρ_ϵ	lag-1 residual autocorrelation
AA **for each light intensity with leaf using agcurve curve parameters**	
$\widehat{\text{AA}}_{klm}$	estimate of AA for the k^{th} leaf at light intensity l in accession m
effects of light intensity, light treatments, and population on AA	
$\beta_{\text{AA},0}$	intercept of AA at low light intensity in shade treatment

$\beta_{\text{AA,2000}}$	effect of high light intensity at PPFD $= 2000\ \mu\text{mol}\,\text{m}^{-2}\,\text{s}^{-1}$ on AA
$\beta_{\text{AA,sun}}$	effect of sun treatment on AA
$\beta_{\text{AA,2000,sun}}$	effect of high light intensity at PPFD $= 2000\ \mu\text{mol}\,\text{m}^{-2}\,\text{s}^{-1}$ on AA in sun treatment
$\vec{\beta}_{\text{AA,acc}}$	vector of n_{acc} phylogenetically structured random accession-level effects on AA; $\vec{\beta}_{\text{AA,acc}} \sim \text{MVN}(\vec{0}, \mathbf{\Sigma}_{\text{AA,acc}})$
$\mathbf{\Sigma}_{\text{AA,acc}}$	$n_{\text{acc}} \times n_{\text{acc}}$ covariance matrix of phylogenetically structured random accession-level effects on AA;
$\vec{\beta}_{\text{AA,rep}}$	vector of n_{rep} random replicate-level effects on AA; $\vec{\beta}_{\text{AA,rep}} \sim \text{Normal}(0, \sigma_{\text{AA,rep}})$
$\vec{\beta}_{\text{AA,2000,acc}}$	vector of n_{acc} phylogenetically structured random accession-level effects of high light intensity at PPFD $= 2000\ \mu\text{mol}\,\text{m}^{-2}\,\text{s}^{-1}$ on AA; $\vec{\beta}_{\text{AA,2000,acc}} \sim \text{MVN}(\vec{0}, \mathbf{\Sigma}_{\text{AA,2000,acc}})$
$\vec{\beta}_{\text{AA,sun,acc}}$	vector of n_{acc} phylogenetically structured random accession-level effects of sun treatment on AA; $\vec{\beta}_{\text{AA,sun,acc}} \sim \text{MVN}(\vec{0}, \mathbf{\Sigma}_{\text{AA,sun,acc}})$
$\sigma_{\text{AA},\epsilon,0}$	intercept of phylogenetically unstructured residual standard deviation of AA
$\beta_{\text{AA},\epsilon,2000}$	effect of high light intensity at PPFD $= 2000\ \mu\text{mol}\,\text{m}^{-2}\,\text{s}^{-1}$ on phylogenetically unstructured residual standard deviation of AA (log-link scale)
$\beta_{\text{AA},\epsilon,\text{sun}}$	effect of sun treatment on phylogenetically unstructured residual standard deviation of AA (log-link scale)
$\sigma_{\text{AA,rep}}$	standard deviation of random replicate-level effects on AA
$\alpha_{\text{AA,acc}}$	decay rate of phylogenetic covariance in random accession-level effects on AA
$\sigma^2_{\text{AA,acc}}$	phylogenetic diffusion rate in random accession-level effects on AA
$\alpha_{\text{AA,2000,acc}}$	decay rate of phylogenetic covariance in random accession-level effects of high light intensity at PPFD $= 2000\ \mu\text{mol}\,\text{m}^{-2}\,\text{s}^{-1}$ on AA
$\sigma^2_{\text{AA,2000,acc}}$	phylogenetic diffusion rate in random accession-level effects of high light intensity at PPFD $= 2000\ \mu\text{mol}\,\text{m}^{-2}\,\text{s}^{-1}$ on AA
$\alpha_{\text{AA,sun,acc}}$	decay rate of phylogenetic covariance in random accession-level effects of sun treatment on AA
$\sigma^2_{\text{AA,sun,acc}}$	phylogenetic diffusion rate in random accession-level effects of sun treatment on AA
effects of native light habitat on population-level AA	
$\beta_{\text{AA,PPFD},0}$	intercept of accession-level AA when native PPFD $= 0\ \mu\text{mol}\,\text{m}^{-2}\,\text{s}^{-1}$
$\beta_{\text{AA,PPFD},1}$	slope of native PPFD on accession-level AA
$\alpha_{\text{AA,PPFD}}$	decay rate of phylogenetic covariance in residuals of model testing effect of native PPFD on accession-level AA
$\sigma^2_{\text{AA,PPFD}}$	phylogenetic diffusion rate in residuals of model testing effect of native PPFD on accession-level AA

A–g_{sw} curve parameters

We modeled $\log(A)$as a quadratic function of $\log(g_{\text{sw}})$for each leaf using the following equation:

$$\log(A_{ij}) = (\beta_0 + b_{0,j}) + (\beta_1 + b_{1,j}) \log g_{\text{sw},i} + (\beta_2 + b_{2,j}) \log {g_{\text{sw},i}}^2 + \epsilon_i$$

where β_0, β_1, and β_2 are the average intercept, linear, and quadratic coefficients, respectively. We used diffuse normal priors with mean 0 and standard deviation 10 on these parameters. We estimated random effects of curve j on the intercept ($b_{0,j}$), linear ($b_{1,j}$), and quadratic ($b_{2,j}$) coefficients. We assumed that the $j \times 3$ array of coefficients was multivariate normal a mean vector of $\vec{0}$ and covariance Σ_{curve}. We used a weakly informative normal prior with mean 0 and standard deviation 1 on the log-transformed standard deviations (i.e. the diagonal of Σ_{curve}). We used a weakly informative LJK(2) prior on the correlation matrix. The off diagonal elements of Σ_{curve} can be calculated from its diagonal elements and the correlation matrix.

The residuals ϵ_i were modeled as a lag-1 autocorrelated time-series. We further assumed that the residual standard deviation of the j^{th} curve ($\sigma_{\epsilon,j}$) was inversely proportional to the leaf surface area (S_j) within the chamber:

$$\log(\sigma_{\epsilon,j}) = \log(\sigma_{6\,\text{cm}^2,\epsilon}) + (6 - S_j)\beta_{S,\epsilon}$$

where $\sigma_{6\,\text{cm}^2,\epsilon}$ is the minimum residual standard deviation when the 6 cm^2 chamber is completely filled. The residual standard deviation increases on log-linear scale by $\beta_{S,\epsilon}$. We used a weakly informative normal prior with mean -3 and standard deviation 5 on $\log(\sigma_{6\,\text{cm}^2,\epsilon})$ and a weakly informative normal prior with mean 0 and standard deviation 1 on $\beta_{S,\epsilon}$.

AA **for each light intensity with leaf using A–g_{sw} curve parameters**

Within the k^{th} leaf, we estimated AA for each light intensity by integrating the difference in $\log(A)$ between the amphi and pseudohypo A–g_{sw} curves over the range of g_{sw} values where the curves overlap (from $\min(\log(g_{\text{sw}}))$ to $\max(\log(g_{\text{sw}}))$). The estimate of AA for the k^{th} leaf at light intensity l in population m is:

$$\widehat{\text{AA}}_{klm} = \int_{\min(\log(g_{\text{sw}}))}^{\max(\log(g_{\text{sw}}))} \log\left(\frac{\hat{A}_{\text{amphi}}(x; \theta_{klm,\text{amphi}})}{\hat{A}_{\text{hypo}}(x; \theta_{klm,\text{hypo}})}\right) dx$$

where:

$$\theta_{\text{amphi}} \in \{\hat{b}_{0,f(\text{amphi},k,l,m)}, \hat{b}_{1,f(\text{amphi},k,l,m)}, \hat{b}_{2,f(\text{amphi},k,l,m)}\}, \text{and}$$

$$\theta_{\text{hypo}} \in \{\hat{b}_{0,f(\text{hypo},k,l,m)}, \hat{b}_{1,f(\text{hypo},k,l,m)}, \hat{b}_{2,f(\text{hypo},k,l,m)}\}.$$

The function $f : \Theta_1 \to \Theta_2$ maps the set Θ_1 indexed by leaf type (amphi or pseudohypo), leaf replicate, light intensity, and population to set Θ_2 indexed by individual A–g_{sw} curve. This mapping is necessary because the random effects structure differs between models of $\log(g_{\text{sw}})$ on $\log(A)$ and that of models predicting AA described in the next section.

Effects of light intensity, light treatment, and population on AA

We tested for effects of light intensity, light treatment, population, and their interactions on AA. All models included effects of light intensity and light treatment, as well as random effects of population and replicate within population. More complex models included interactions between light intensity and light treatment, as well as random effects of population on the effects of light intensity and light treatment. We used a weakly informative normal prior with mean 0 and standard deviation 10 for fixed effects of light intensity and treatment. We used a weakly informative normal prior with mean -3 and standard deviation 5 for the the random effect standard deviation of replicate within population. We accounted for the phylogenetic structure among the random effects of population using an Ornstein-Uhlenbeck (OU) process (*66*). The expected covariance between populations i and j (Cov(i, j)) is:

$$\text{Cov}(i, j) = \frac{\sigma^2}{2\alpha} \exp(-\alpha D_{ij})$$

where σ^2 is the variance of the random effect, α is the rate of decay of the covariance with phylogenetic distance, D_{ij}, the phylogenetic distance between populations i and j. We estimated $\sigma^2/(2\alpha)$ and α as a separate parameters and reparameterized them as σ^2 and α. We used a weakly informative normal prior with mean 0 and standard deviation 10 on OU parameters.

We modeled the residual standard deviation of AA, (i.e. phylogenetically unstructured variation unaccounted for by explanatory variables) on a log-link scale with effects of light intensity and light treatment. We used a weakly informative normal prior with mean -3 and standard deviation 5 on the residual standard deviation intercept and a weakly informative normal prior with mean 0 and standard deviation 1 on the effects of light intensity and light treatment on the residual standard deviation.

Effects of native light habitat on population-level AA

We tested a linear effect of native light habitat on population-level AA. In Models 1 and 2, we used the random intercept of AA as a response variable; in model 3 we used the random intercept plus the random effect of population at high light intensity; in model 4 we used the random intercept plus the random effect of population in the sun treatment; in model 5 we used the random intercept plus the random effects of population at high light intensity and sun treatment. We used a weakly informative normal prior with mean 0 and standard deviation 1 for the slope and intercept. We accounted for the phylogenetic structure among the model residuals using an (OU) process. We used a weakly informative normal prior with mean 0 and standard deviation 10 on OU parameters.

Predictions

The assimilatory, plastic, and constitutive hypotheses make different predictions about the relationship between AA and light intensity, light treatment, and native PPFD among populations. Since these hypotheses are not mutually exclusive, we describe how we assessed support for one, two, or all three hypotheses simultaneously in Table S6. In general, the assimilatory hypothesis was supported if AA was greater at high light intensity than low light intensity. The plastic hypothesis was supported if AA

was greater in sun leaves than shade leaves. The constitutive hypothesis was supported if population-level AA increased with native PPFD. In interactive models, we only consider positively reinforcing interactions between high light intensity, sun leaves, and native PPFD because these are the only interactions which could explain why amphistomatous leaves are advantageous in high light habitats.

We evaluated predictions using a combination of parameter estimation and model selection. In all cases, we estimated parameters and confidence intervals as described in Section . If the 95% confidence intervals for a parameter did not overlap zero, we considered the parameter to be significantly different from zero. We used the leave-one-out cross-validation information criterion (LOOIC) to compare the fit of models (Table S4) using the *R* package **loo** version 2.8.0 (*67*) to calculate LOOIC values. Note that LOOIC was calculated only from pointwise likelihood values of the submodel estimating effects of light intensity, light treatments, and population on AA (see Section). We considered models with two standard errors of the mean lower LOOIC value to be a better fit to the data; we considered models with LOOIC values within two standard errors of the mean to be have similar support.

Table S6: Predictions of competing hypotheses about the relationship between AA and light intensity, light treatment, and native PPFD among populations. The middle column lists specific directional predictions about parameter values and model fit according to leave-one-out cross-validation information criterion (LOOIC), where LOOIC_i is the LOOIC value for model i. The rightmost column describes the predictions in words and explains how population-level AA is calculated in the relevant model.

Hypothesis	**Prediction(s)**	**Description**
Assimilatory	$\beta_{\text{AA,2000}} > 0$	Average AA at high light intensity is greater than that at low light intensity
Plastic	$\beta_{\text{AA,sun}} > 0$	Average AA in sun leaves is greater than that in shade leaves
Constitutive	$\beta_{\text{PPFD,AA}} > 0$	Population-level AA (AA_{acc}) increases with native PPFD $\text{AA}_{\text{acc}} = \beta_{\text{AA},0} + \vec{\beta}_{\text{AA,acc}}$
Assimilatory × Plastic	$\beta_{\text{AA,2000,sun}} > 0$ $\text{LOOIC}_1 > \text{LOOIC}_2$	Average AA is highest at high light intensity in sun leaves
Assimilatory × Constitutive	$\beta_{\text{AA,2000}} > 0$ $\beta_{\text{PPFD,AA}} > 0$ $\text{LOOIC}_1 > \text{LOOIC}_3$	Average AA at high light intensity is greater than that at low light intensity Population-level AA at high light intensity ($\text{AA}_{\text{acc,2000}}$) increases with native PPFD $\text{AA}_{\text{acc,2000}} = \beta_{\text{AA},0} + \vec{\beta}_{\text{AA,acc}} + \vec{\beta}_{\text{AA,2000,acc}}$

Plastic × Constitutive	$\beta_{\text{AA,sun}} > 0$	Average AA in sun leaves is greater than that in shade leaves
	$\beta_{\text{PPFD,AA}} > 0$	Population-level AA in sun leaves ($\text{AA}_{\text{acc,sun}}$) increases with native PPFD
	$\text{LOOIC}_1 > \text{LOOIC}_4$	$\text{AA}_{\text{acc,sun}} = \beta_{\text{AA,0}} + \vec{\beta}_{\text{AA,acc}} + \vec{\beta}_{\text{AA,sun,acc}}$
Assimilatory × Plastic × Constitutive	$\beta_{\text{AA,2000,sun}} > 0$	Average AA is highest at high light intensity in sun leaves
	$\beta_{\text{PPFD,AA}} > 0$	Population-level AA at high light intensity in sun leaves ($\text{AA}_{\text{acc,2000,sun}}$) increases with native PPFD
	$\text{LOOIC}_3 > \text{LOOIC}_5$	$\text{AA}_{\text{acc,2000,sun}} = \beta_{\text{AA,0}} + \vec{\beta}_{\text{AA,acc}} + \vec{\beta}_{\text{AA,2000,acc}} + \vec{\beta}_{\text{AA,sun,acc}}$

Results

- Variation in stomatal ratio among pops and light treatments
- Table S7: Model comparison LOOIC tables
- Table S8: Model comparison LOOIC tables with LMA
- Table S9: Calculation of alternate scenario where amphi leaves can get same A with less R